Fachtagung "Experimentelle Strömungsmechanik"
6. – 8. September 2016, Cottbus

Interagierende Trägheitsmoden in einem differenziell rotierenden Kugelspaltexperiment

Interacting inertial modes in a differentially rotating spherical gap flow experiment

Michael Hoff[1], Uwe Harlander[1], Christoph Egbers[1], Santiago A. Triana[2]
[1] Lehrstuhl für Aerodynamik und Strömungslehre, Brandenburgisch Technische Universität Cottbus - Senftenberg
[2] Royal Observatory of Brussels, Belgien

geo- und astrophysikalische Strömung, Wellen in rotierenden Fluiden, Instabilität
geo- and astrophysical flows, waves in rotating fluids, instability

Abstract

Inertial modes are Coriolis-restored linear wave modes that arise in rapidly rotating fluids. Recent experimental works showed that inertial modes exist in differentially rotating spherical gap flows [1,2]. It is an open issue why only a few modes develop and how they get enhanced.
We present a study of inertial modes in the Cottbus' spherical gap apparatus (Fig. 1), where the inner sphere is slower- or counter-rotating with respect to the outer shell. The Rossby number $Ro = (\Omega_{in} - \Omega_{out}) / \Omega_{out}$, with Ω_{in} and Ω_{out} the inner and outer sphere rotation rate, characterizes the flow. We use a simple Particle-Image-Velocimetry (PIV) system in the rotating frame of the outer shell to visualize the flow in the gap [3]. Since most of the previous spherical shell experiments are without optical access, our method gives us new qualitative and quantitative insights into the flow between concentric spheres. With that we are able to show for the first time quantitative horizontal velocity fields of the inertial modes in a differentially rotating spherical gap experiment. We compare the uniquely identified modes with the literature [1,2] and, moreover, we confirm that the experimentally obtained modes are indeed similar to their analytic full-sphere counterparts derived by Zhang et al. 2001 [4].

Introduction

Spherical gap flows are omnipresent in nature. The atmosphere and the ocean form very thin spherical gaps, whereas the Earth's solid iron inner core and the lower mantle form a thick spherical gap where the molten metal of the liquid outer core represents the fluid in between. A characteristic feature of spherical gaps is that the inner sphere and the outer shell can rotate at different speeds, i.e. differential rotation, or nominally the spherical Couette flow. This strongly effects the liquid interior. Therefore, spherical gap flow models and laboratory experiments are often used to understand dynamics and mechanisms in planets and stars, as well as ocean and atmosphere.

Karlsruhe, Germany, ISBN 978-3-9816764-2-6

Common features in rapidly rotating systems, i.e. when the rotation dominates the viscosity, are inertial waves which are Coriolis-restored internal oscillations. If no boundaries are considered, inertial waves exist at any frequency ω in the interval $0 \le \omega \le 2\Omega_{out}$, where Ω_{out} is the rotation speed of the outer shell. The frequency of a plane inertial wave is given by the dispersion relationship

$$\omega = 2\Omega_{out}\sqrt{\frac{m^2}{k^2+l^2+m^2}} = 2\Omega_{out}\cos\theta, \qquad (1)$$

where $\mathbf{k} = (k,l,m)$ is the wave vector and θ is the angle between the horizontal plane and the group velocity $\mathbf{c_g} = \partial\omega/\partial\mathbf{k}$, showing the direction of energy propagation. From (1), it is obvious that the frequency of inertial waves does *not* depend on the magnitude of the wave vector but only on its direction. This means that for low frequencies the inertial wave shear layers are parallel to the rotation axis and for high frequencies perpendicular to it.

One striking property of plane inertial waves, which they share also with internal gravity waves, is their reflection behavior at solid boundaries. If an incident wave ray hits a sloping boundary, it will be reflected in the same angle with respect to the rotation axis. This can lead to energy focusing and eventually to attractors or closed orbits [3].

The Poincaré equation for inertial waves is hyperbolic which does not comply with the boundary conditions. The problem becomes mathematically ill-posed and, for an inviscid fluid, solutions are generally singular. An exception has been found by Zhang et al. 2001 for full sphere geometry [4].

In contrast to full sphere geometry, in spherical gap geometry no analytic solution for inertial modes could be found in spite of the similarity between both geometries. Rieutord et al. 2012 [2] postulate that most of the fluid volume in a spherical gap (~85% with $\eta = r_{in}/r_{out} = 1/3$) lies outside the tangent cylinder (vertical shear layer touching the inner spheres equator [5]) and is in solid-body rotation with the outer shell Ω_{out}. Due to this fact, they conclude that there might be a structural similarity between the full-sphere [4] and the spherical-gap inertial modes. To this day, there was no quantitative confirmation of the structural similarity in laboratory experiments.

Our experiments reveal a number of distinct inertial modes excited by differential rotation. We will not focus on the excitation mechanism itself (for this purpose see [1,2]). We rather use the decisive advantage of a full optical access, and a visualization of the horizontal plane up to 40%, to compare the velocity fields of distinct inertial modes with the velocity fields of the analytic full-sphere modes [4] and, moreover, to confirm that, indeed, most of the fluid volume outside the tangent cylinder rotates with Ω_{out}.

Experimental set-up

The experimental apparatus (Fig. 1) consists of two independently rotating concentric spheres with an inner sphere radius of $r_{in} = 40\,\text{mm}$ and an outer radius of $r_{out} = 120\,\text{mm}$. From this follows a gap width of $d = 80\,\text{mm}$ and a radius ratio of $\eta = r_{in}/r_{out} = 1/3$. The inner sphere is made of black anodized aluminum, suspended on a shaft of diameter 14 mm to ensure an axisymmetric rotation. The outer shell is made of acrylic glass. The working fluid is

Karlsruhe, Germany, ISBN 978-3-9816764-2-6

a silicone oil of viscosity $\nu = (0.65 \pm 0.07)\,\mathrm{mm}^2/\mathrm{s}$. To avoid optical distortions due to the curvature of the outer shell, the entire shell is immersed into a cubic tank of de-ionized water. If we use $(\Omega_{in} - \Omega_{out}) r_{out}$ as velocity scale, the characteristic Rossby number is defined by $Ro = (\Omega_{in} - \Omega_{out}) / \Omega_{out}$. Further, the Ekman number $E = \nu / (\Omega_{out} r_{out}) \geq 6.8 \cdot 10^{-6}$ characterizes the ratio between viscosity and Coriolis forces. More information about the apparatus can be found in [3,6].

For visualization in the meridional plane, the flow was seeded by Kalliroscope tracer particles and illuminated using a vertical laser light sheet technique (Fig. 2a). Because of their platelike shape, the particles are aligned with the shear flow showing bright and dark portions of reflection. A camera recorded the flow in the laboratory frame perpendicular to the laser sheet. The flow in the horizontal plane has been studied quantitatively with particle image velocimetry (PIV) with spherical hollow glass spheres as tracer particles (Fig. 2b). Two GoPro Hero 4 cameras immersed in the water as well, offering a cheap alternative to enable high-resolution recordings, observed the particle motion in the frame at rest with the outer shell. With this setup, up to 40% of the horizontal plane can be observed.

The calibration of the PIV setup is rather complicated since we have a complex and closed system and cannot directly calibrate during the measurements. The setup in Fig. 2c shows a proper alternative for the calibration of the PIV. For the respective measurement height, a black circle area with markers, representing the world coordinates with known distances, has been fixed at the bottom of the aquarium. The Camera was fixed from above with the optical path perpendicular to the object, in the same distance as in the real experiments. Then, we filled the aquarium with water until the lens of the camera immersed into the water. The camera has been adjusted until we observe the same situation like in the real experiments. The obtained image of the world coordinates represents the input file for the Matlab toolbox matPIV v.1.6.1 [7] to transform the pixel coordinates of the recorded image to the real Cartesian coordinates. We validated this transformation with measurements of solid-body rotation from which we know the corresponding analytical velocity field. The errors in the center of the field of view are between 8% to 15%, and around 20% to 25% in the corners and edges.

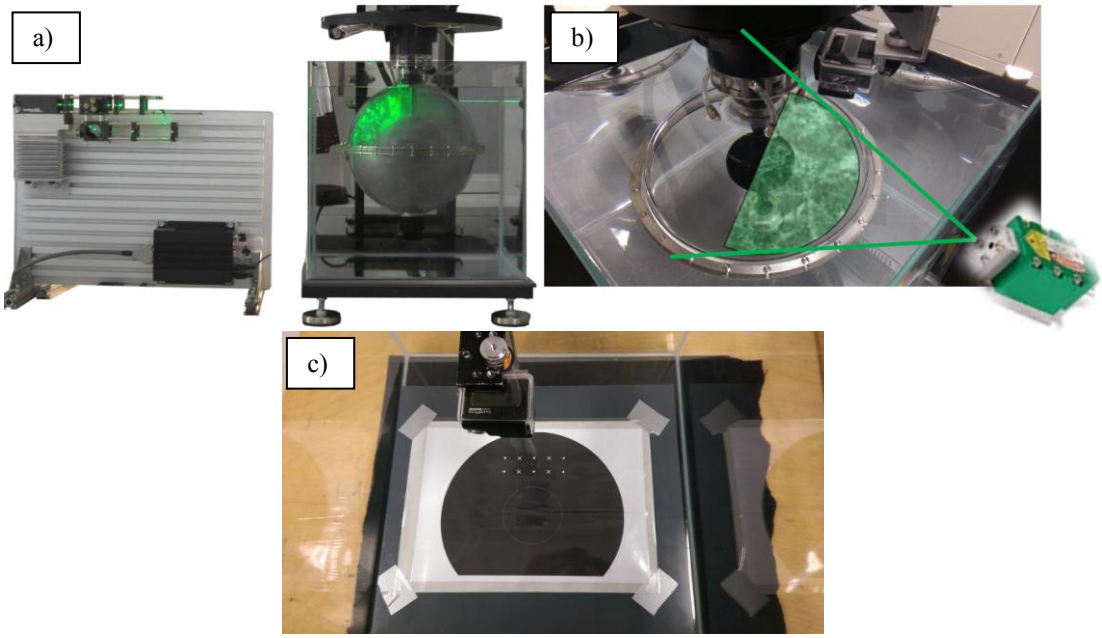

Fig. 2: a) Setup for measurements in the meridional plane. b) Setup for measurements in the horizontal plane. c) Setup of the calibration for PIV

Data and data processing

We performed particular ramps for two fixed $\Omega_{out} = (30,60)$ rounds per minute (rpm). The inner sphere rotation has been varied between $-45 \le \Omega_{in} \le +24$ and $-90 \le \Omega_{in} \le +48$ for the respective Ω_{out} so that we cover $-2.5 \le Ro \le -0.2$ in the Rossby number space, with a resolution of $\Delta Ro \approx 1/30$. At each particular step, we waited 5 min to ensure an equilibrium state $(E^{-1/2}\Omega_{out}^{-1} \propto 1-2\,\mathrm{min})$ and recorded the flow for 15 min in a horizontal plane at height 4cm above the equator.

The movies in the horizontal plane have been converted into gray scale images and analyzed by using the Matlab toolbox matPIV v.1.6.1 [7]. For the present purpose, a spatial resolution of 1920x1080 pixels was sufficient to obtain reliable velocity fields. The sampling rate varies from 1/15s to 1/60s depending on the expected velocity magnitudes. We used three interrogation steps from 128x128 to 64x64 to a final window size of 32x32 pixels with an overlap of 0.5. A signal-to-noise filter, a peak height filter and a global filter that removes vectors significantly larger or smaller than the majority of vectors, have further been applied. A Fourier analysis was applied to the velocity components (u,v) to detect dominant frequencies in the flow. For these frequencies, which usually represent inertial modes, the corresponding flow patterns have been studied by a harmonic analysis. The harmonic analysis is a signal-demodulation technique in which the user specifies wave frequencies to be analyzed and applies least-square techniques to find the unknown amplitudes and phases of the waves [8].

Results

We start by discussing the time-averaged velocity profiles. Fig. 3 shows the azimuthally averaged azimuthal mean flow for four different Rossby numbers $Ro = -(0.25,0.65,1.37,1.76)$ (colors and labeled) as a function of radius. The velocities are measured in the frame rotating with the outer shell. Therefore, the highest velocity is found to be inside the tangent cylinder (dashed line) above the differentially rotating inner sphere (note that the flow is retrograde). Moving outwards, the velocity is rapidly dropping down to almost zero (the Stewartson shear layer [5]) and remains constant for $r/r_{out} > 0.5$. The most surprising fact in Fig. 3 is that the shear layer where the fluid velocity drops down is significantly shifted outwards compared to the location of the tangent cylinder where it was originally expected from [2]. Moreover, this intrusion of velocity into the bulk increases with decreasing Rossby number. What makes a comparison with analytic approximations difficult is that we are not in the Rossby number regime $|Ro| << 1$ for which the theory holds. Therefore, we think that the strongly differentially rotating inner core has a much higher impact on the flow behavior than traditionally expected. However, the largest portion of fluid outside the tangent cylinder is indeed in solid-body rotation with Ω_{out} which is in agreement to the assumptions of Rieutord et al. [2].

Karlsruhe, Germany, ISBN 978-3-9816764-2-6

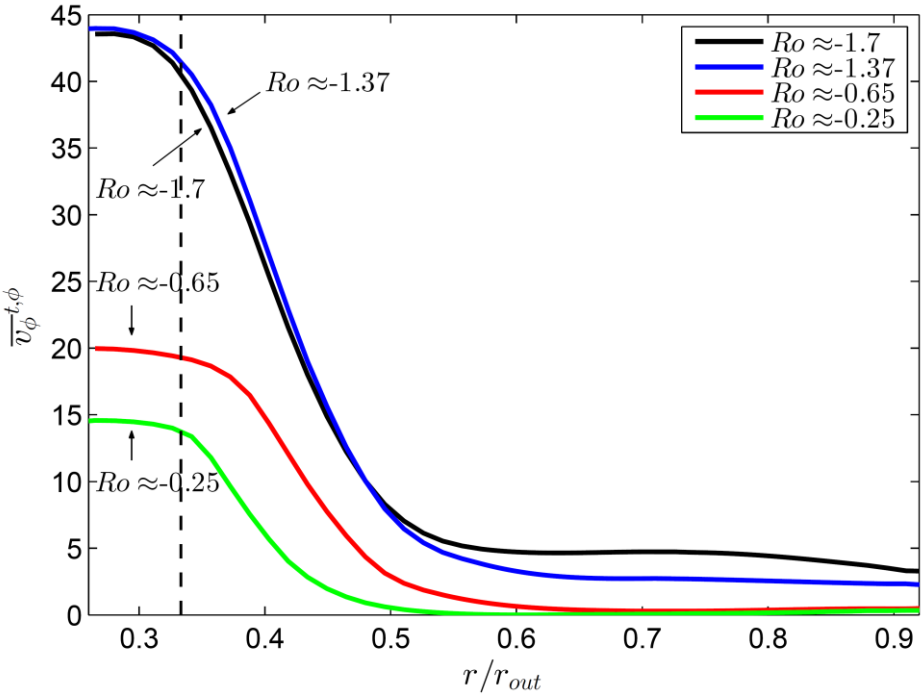

Fig. 3: Azimuthally averaged azimuthal velocity for $\Omega_{out} = 60\mathrm{rpm}$, $E = 0.67 \cdot 10^{-5}$ for four different Rossby numbers (colors) as a function of the radius. The dashed vertical line marks the position of the tangent cylinder.

Fig. 4 shows the amplitude spectra in log-log scale for $\Omega_{out} = 60\mathrm{rpm}$, $E = 0.67 \cdot 10^{-5}$ for the same four Rossby numbers $Ro = -(0.25, 0.65, 1.37, 1.76)$. Generally, it can be seen that the background noise level increases with decreasing Rossby number, since the strength of the differential rotation and the wave activities increase. In particular, the spectra reveal different peaks, depending on the respective Rossby number. We found that these peaks correspond with distinct inertial modes (see labels which will be explained in the following).

We use the following notation to determine the modes. Assuming that the patterns of the modes have structural similarities to the modes from previous studies, each mode can be identified in terms of spherical harmonics Y_l^m with degree l and order m. Further each mode has a frequency $\hat{\omega} = \omega / \Omega_{out}$. This notation $(l, m, \hat{\omega})$ has been used in any of the previous studies [1,2,4,11,12].

In order to get a first impression of the corresponding patterns, we extracted the most dominant frequencies out of the spectra (Fig. 4) and filtered the velocity data for the extracted frequencies with the help of the harmonic analysis. The left column of Fig. 5 displays the harmonically filtered instantaneous velocity fields (mm/s) of the three most dominant frequencies $\hat{\omega} = (0.70, 0.08, 0.62)$ for the 60rpm ramp. All the shown patterns propagate retrograde, i.e. against the rotation of the outer shell. From these figures, we can derive the azimuthal wavenumbers m visually: in case the vectors at the left and right hand side point in opposite directions, the mode has wavenumber $m = 2$; in case they point in the same direction, the mode has wavenumber $m = 1$. Therefore, the three modes shown have wavenumbers $m = (2,1,1)$. A further cross-correlation of the velocity time series for different positions in the gap confirms the obtained wavenumbers.

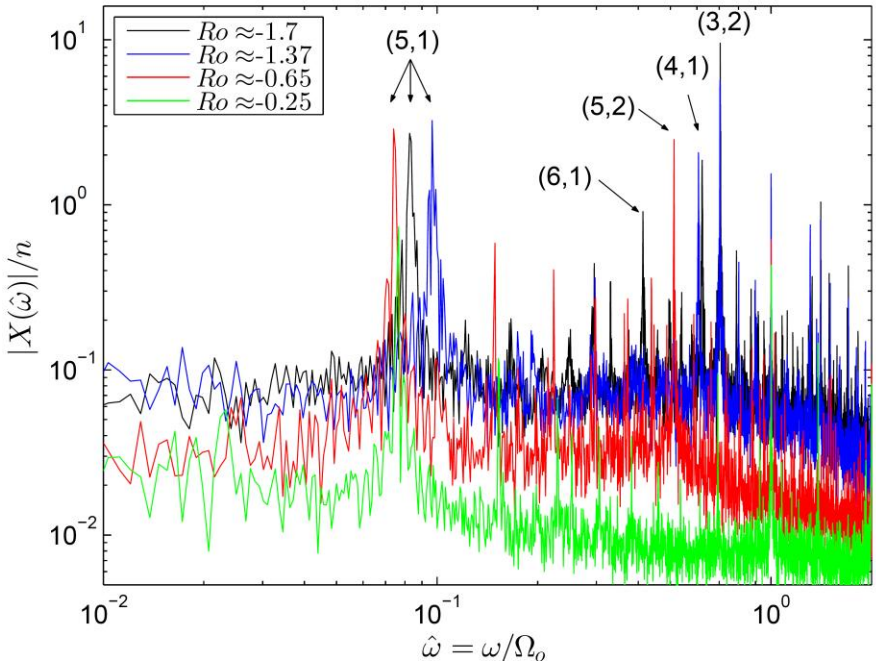

Fig. 4: Amplitude spectra for $\Omega_{out} = 60\mathrm{rpm}$, $E = 0.67 \cdot 10^{-5}$ for four different Rossby numbers (colors) as a function of $\hat{\omega} = \omega / \Omega_{out}$ in the inertial wave range. The labels show inertial modes.

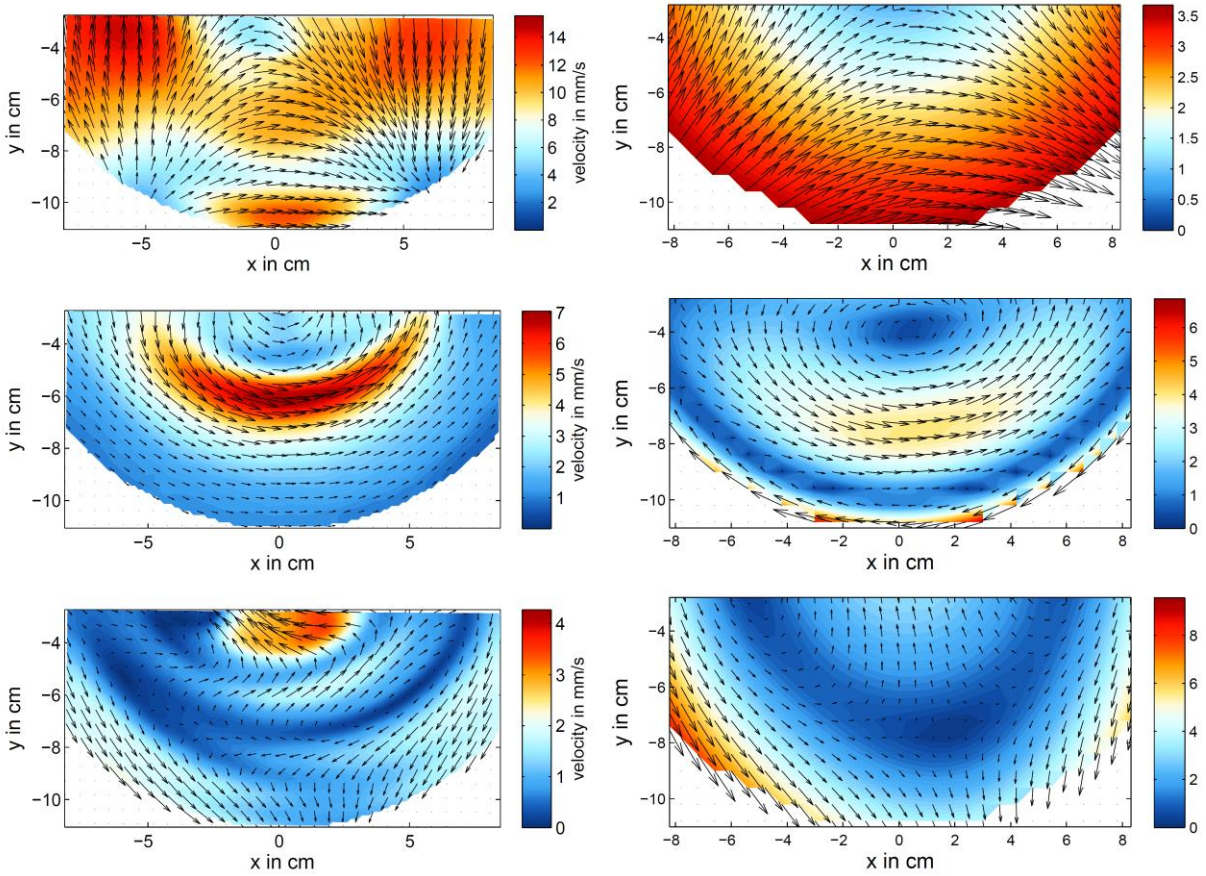

Fig. 5: Left column: Measured instantaneous velocity (mm/s) at 4cm above the equator, filtered by the harmonic analysis for the parameters $\Omega_{out} = 60\mathrm{rpm}$, $E = 0.67 \cdot 10^{-5}$, $Ro = -1.67$; inertial mode (3,2,0.71) (upper), (5,1,0.08) (middle) and (4,1,0.62) (lower). Right column: The corresponding analytic full-sphere instantaneous velocity fields (arbitrary units) from Zhang et al. 2001 [7] (see also Tab. 1).

To determine the l number, we did a qualitative comparison to the analytic model of full-sphere modes by Zhang et al. 2001 [4]. The right column of Fig. 5 shows the analytic full-sphere modes $(l,m,\hat{\omega}) = [(3,2,0.6667),(5,1,-0.0682),(4,1,0.6120)]$, which agree surprisingly well with our experimental modes $(l,m,\hat{\omega}) = [(3,2,0.70),(5,1,0.08),(4,1,0.62)]$. Note that we measured in proximity to the inner sphere's north pole so that boundary layer effects cannot be excluded and might lead to differences. With this procedure, we uniquely determined two more modes $(l,m,\hat{\omega}) = [(6,1,0.41),(5,2,0.52)]$ labeled in Fig. 4. Table 1 gives a summary of the detected wave modes and their comparison to previously detected modes.

Tab. 1: Uniquely identified inertial modes. Identification by comparison with the analytic model [4] and the experimental works from [2,12]. The abbreviations mean: ES - equatorial symmetric, EA - equatorial antisymmetric, SL - Stewartson-layer instability, taken from [11]. The values with subscript 'Triana' are taken from [12]. Note that the (5,1) mode is the low-frequency columnar Rossby mode [3].

(a) $\Omega_{out} = 30\text{rpm}, E = 1.35 \cdot 10^{-5}$

(l,m)	$\hat{\omega}_{ana}$	$\hat{\omega}_{meas}$	$\hat{\omega}_{Triana}$	$\lvert Ro_{meas} \rvert$	$\lvert Ro_{Triana} \rvert$	Inst.
(3,2)	0.6667	$0.715 - 0.698$	$0.760 - 0.700$	$1.989 - 0.945$	$1.25 - 0.70$	*SL, EA*
(4,1)	0.6120	$0.615 - 0.591$	$0.639 - 0.605$	$1.989 - 1.041$	$2.20 - 1.42$	*SL, EA*
(5,1)	-0.0682	$0.140 - 0.081$	~ 0.1	$1.989 - 0.252$	< 1.4	*SL, ES*
(5,2)	0.4669	$0.529 - 0.515$	$0.573 - 0.508$	$0.693 - 0.631$	$0.77 - 0.50$	*SL, EA*
(6,1)	0.4405	$0.429 - 0.403$	$0.500 - 0.444$	$1.989 - 1.583$	$1.4 - > 0.8$	*SL, EA*

(b) $\Omega_{out} = 60\text{rpm}, E = 0.67 \cdot 10^{-5}$

(l,m)	$\hat{\omega}_{ana}$	$\hat{\omega}_{meas}$	$\hat{\omega}_{Triana}$	$\lvert Ro_{meas} \rvert$	$\lvert Ro_{Triana} \rvert$	Inst.
(3,2)	0.6667	$0.708 - 0.688$	$0.760 - 0.700$	$1.727 - 0.888$	$1.25 - 0.70$	*SL, EA*
(4,1)	0.6120	$0.625 - 0.596$	$0.639 - 0.605$	$1.727 - 0.888$	$2.20 - 1.42$	*SL, EA*
(5,1)	-0.0682	$0.108 - 0.074$	~ 0.1	$1.727 - < 0.2$	< 1.4	*SL, ES*
(5,2)	0.4669	$0.536 - 0.508$	$0.573 - 0.508$	$0.729 - 0.600$	$0.77 - 0.50$	*SL, EA*
(6,1)	0.4405	$0.414 - 0.407$	$0.500 - 0.444$	$1.727 - 1.540$	$1.4 - > 0.8$	*SL, EA*

The most remarkable differences between the experimental spherical shell modes and the analytic full-sphere modes are: i) the frequency of the experimental spherical shell modes is mostly slightly higher than for the analytic modes. This is due to the presence of the inner sphere as it was already reported by Aldridge 1967 [9]. He reported that the frequency shift becomes larger when the aspect ratio of the spherical gap increases. However, the agreement to the experiments conducted by Triana [12] is fairly well, in particular for the (3,2), (5,2) and the (5,1) mode (see Tab. 1). ii) In contrast to the others, the (5,1) mode has an axisymmetric shape and could be identified as the first Stewartson-layer instability which sets in after solid-body rotation [10,11]. The negative analytic frequency in the full sphere means that this mode is propagating prograde. In contrast, in a spherical gap, the direction of propagation changes its sign and becomes retrograde. This fact arises due to the β-effect which has different signs left and right hand side of the tangent cylinder (see [3] for detailed information).

Karlsruhe, Germany, ISBN 978-3-9816764-2-6

Summary

In this study, we presented experimental results of a differentially rotating spherical gap flow with Ekman numbers $E \geq 0.67 \cdot 10^{-5}$ and $-2.5 \leq Ro \leq -0.2$ (the inner sphere is rotating slower or counter-rotates to the outer shell). The full optical access of the experiment gave us the opportunity, for the first time, to get quantitative insights about the structure of inertial modes excited by differential rotation. We compared them carefully with previous findings, experimentally [1,2,12] and, in particular, analytically from a full sphere model [4].

We found that, indeed, a large portion of the fluid outside the tangent cylinder is in solid-body rotation with the outer shell. Due to this fact, we detected a clear structural similarity between our experimental inertial modes and the analytic full-sphere modes, as long as there is no strong velocity component inside the tangent cylinder. Moreover, in agreement to [2], we found that all of our modes are nonaxisymmetric and antisymmetric with respect to the equator, except the columnar Rossby mode [3]. This could be confirmed by Kalliroscope visualization in the meridional plane. All of the detected modes propagate retrograde (against the rotation of the outer shell). An exception compared to the analytic modes is the columnar Rossby mode which propagates retrograde only in a spherical shell and prograde in a full sphere.

Acknowledgements

MH thanks the DFG for funding (HA 2932/7-1). S. A. Triana thanks the European Commission for funding his study in Cottbus via the infrastructure program EuHIT. We acknowledge Adrian Mazilu from the Transilvania University of Brasov for performing most of the experiments in the frame of a Traineeship ERASMUS+ program.

Literature

[1] **Kelley, D.H., Triana, S.A., Zimmerman, D.S., Lathrop, D.P., 2010**: "Selection of inertial modes in spherical Couette flow", Phys. Rev. E., Vol. 81, 026311.
[2] **Rieutord, M., Triana, S.A., Zimmerman, D.S., Lathrop, D.P., 2012**: "Excitation of inertial modes in an experimental spherical Couette flow", Phys. Rev. E, Vol. 86, 026304.
[3] **Hoff, M., Harlander, U., Egbers, Ch., 2016**: "Experimental survey of linear and nonlinear inertial waves and wave instabilities in a spherical shell", J. Fluid Mech.,Vol. 789, 589-616.
[4] **Zhang, K., Earnshaw, P., Liao, X., Busse, F. H. 2001**: "On inertial waves in a rotating fluid sphere", J. Fluid Mech., Vol. 437, 103-119.
[5] **Stewartson, K**.: "On almost rigid rotations. Part 2", J. Fluid Mech., Vol. 26, 131-144.
[6] **Koch, S., Harlander, U., Egbers, Ch., Hollerbach, R. 2013**: "Inertial waves in a spherical shell induced by librations of the inner sphere: experimental and numerical results", Fluid Dyn. Res., Vol. 45, 035504.
[7] **Sveen, J. K**. 2004: "An introduction to MatPIV v.1.6.1".
[8] **Emery, W. J., Thomson, R. E. 2001**: "Data analysis methods in physical oceanography", 2nd ed., Elsevier, Amsterdam and New York.
[9] **Aldridge, K. D.1967**: "An experimental study of axisymmetric inertial oscillations of a rotating liquid sphere", Ph.D. thesis, Massachusetts Institute of Technology.
[10] **Hollerbach, R. 2003**: "Instabilities of the Stewartson layer Part 1. The dependence on the sign of Ro", J. Fluid Mech., Vol. 492, 289-302.
[11] **Wicht, J. 2014**: "Flow instabilities in the wide-gap spherical Couette system", J. Fluid Mech., Vol. 738, 184-221.
[12] **Triana, S. A. 2011**: "Inertial waves in a laboratory model of the Earth's core", Ph.D. thesis, University of Maryland.

Karlsruhe, Germany, ISBN 978-3-9816764-2-6